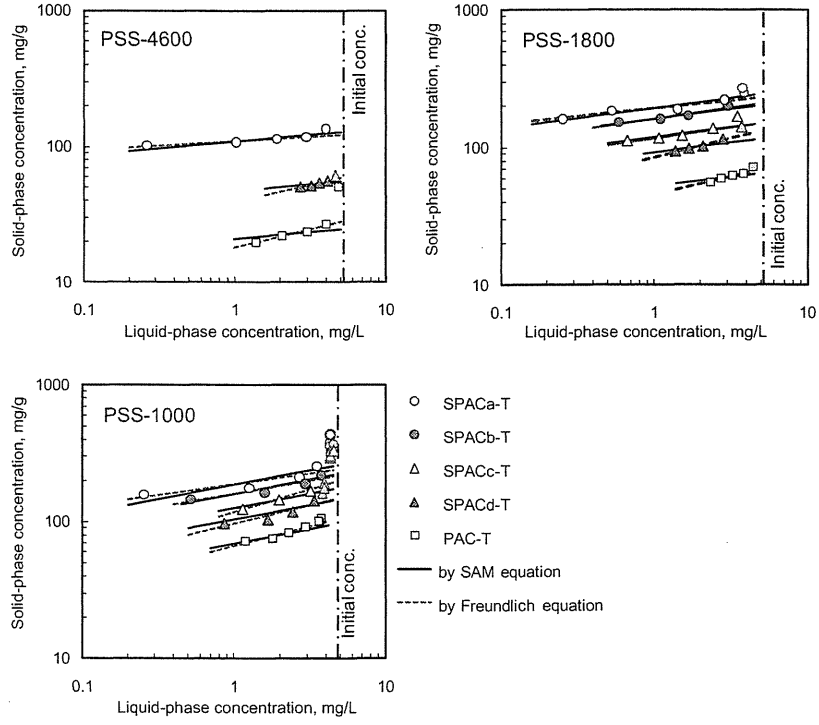

Fig. 1 – Adsorption isotherms of PSS-4600 (upper left panel), PSS-1800 (upper right panel), and PSS-1000 (lower panel). Lines are SAM and Freundlich fits to data (plots close to the initial concentration are red-colored) (For interpretation of the references to colour in this figure legend, the reader is referred to the web version of this article).

capacity on SPACa-T (d_{50} = 0.7 μm), which had the smallest particle size, was highest, followed by SPACb-T (d_{50} = 1.1 μm), SPACc-T (1.9 μm), SPACd-T (3.0 μm), and PAC-T (11.8 μm), in increasing order of particle size: d_{50} is a volumetric median particle diameter, and q_{50} is defined as the amount adsorbed on activated carbon in equilibrium with 2.5 mg/L liquid-phase concentration equal to half the initial concentration (5 mg/L) in the adsorption experiment. Ando et al. (2010) hypothesize that the increase in adsorption capacity with decreasing adsorbent particle size is attributable to molecules adsorbing principally in the exterior region close to the external particle surface. The specific external surface area (surface area per unit mass) available for adsorption would be greater for smaller adsorbent particles, and hence adsorption capacity could be larger on SPAC, which had a much smaller particle size than PAC.

In adsorption isotherm model equations, such as the Freundlich equation, amount adsorbed is expressed as mass of adsorbate per unit mass of adsorbent (e.g., Sontheimer et al., 1988). This relationship implicitly assumes that adsorption surface area is proportional to mass of adsorbent and that adsorption capacity is independent of adsorbent particle size. In a previous study (Karanfil et al., 1996a), the Freundlich equation has been employed successfully to describe adsorption isotherms of PSSs, but the effect of adsorbent size was not studied. In our current research, we

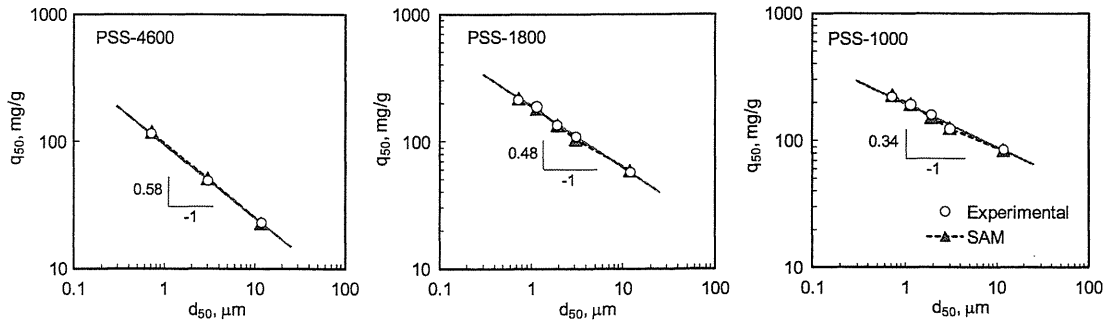

Fig. 2 – PSS adsorption capacities represented by q_{50} against volumetric median diameters of adsorbents. q_{50} is defined as the amount adsorbed on activated carbon in equilibrium with 2.5 mg/L liquid-phase concentration equal to half of initial concentration (5 mg/L) in the adsorption experiment.

have modified the Freundlich equation, as per Eq. (1), in order to describe adsorption capacity dependence on adsorbent particle size, as follows:

$$q_E = KC_E^{1/n} \quad (1)$$

where q_E is the amount adsorbed in solid-phase in equilibrium with liquid-phase concentration (mg/g), C_E is the liquid-phase concentration (mg/L), K is the Freundlich adsorption capacity parameter (mg/g)/(mg/L)$^{1/n}$, and n is the Freundlich exponent.

Beginning with the Freundlich approach, we have modeled the mechanism of Ando et al. (2010) such that the adsorption capacity parameter K is assumed to decrease with increasing distance from the adsorbent particle surface. Using radial coordinates, the Freundlich adsorption capacity parameter is a function of radial distance and particle radius; adsorption capacity of an adsorbent with radius R at radial distance r is then given by Eq. (2), as follows:

$$q_S(r,R) = K_S(r,R)C_E^{1/n} \quad (2)$$

where r is the radial distance from the center of a PAC particle (μm), R is the adsorbent particle radius (μm), $q_S(r, R)$ is the local solid-phase concentration (mg/g) at radial distance r in an adsorbent with radius R, and $K_S(r, R)$ is the radially changing Freundlich adsorption capacity parameter (mg/g)/(mg/L)$^{1/n}$ as a function of radial distance r and adsorbent radius R. Spherical particles were assumed for the PAC and the SPACs, which is the conventional practice for adsorption kinetic models (e.g., Sontheimer et al., 1988).

Therefore, adsorption capacity of an adsorbent with particle radius R in equilibrium with liquid-phase concentration C_E is given by Eq. (3), as shown below:

$$\int_0^R q_S(r,R)\frac{3r^2}{R^3}dr = C_E^{1/n}\frac{3}{R^3}\int_0^R K_S(r,R)r^2dr \quad (3)$$

Accordingly, when the adsorbent size is not uniform, the overall adsorption capacity of the adsorbent is given by Eq. (4), as follows

$$q_E = C_E^{1/n}\frac{3}{R^3}\int_0^\infty\left[\int_0^R K_S(r,R)r^2dr\right]f_R(R)dR \quad (4)$$

where q_E is the overall adsorption capacity of adsorbent (mg/g), and $f_R(R)$ is the normalized particle size distribution function of adsorbent (μm^{-1}).

As a model for $K_S(r, R)$, we adopted Eq. (5), in which adsorption capacity linearly decreases with distance from the external surface to a depth, δ, but thereafter some of the adsorption capacity remains at a level, p, inward from that depth, as depicted in Fig. 3:

$$K_S(r,R) = K_0\left[\max\left(\frac{r-R+\delta}{\delta},0\right)(1-p)+p\right] \quad (5)$$

where K_0 is the Freundlich parameter of adsorption at the external particle surface (K_0 means solid-phase concentration at $r = R$ at unity equilibrium concentration, (mg/g)/(mg/L)$^{1/n}$), δ is the penetration depth (or thickness of the penetration shell, μm), and p is a dimensionless parameter that defines availability of internal porous structures for adsorption.

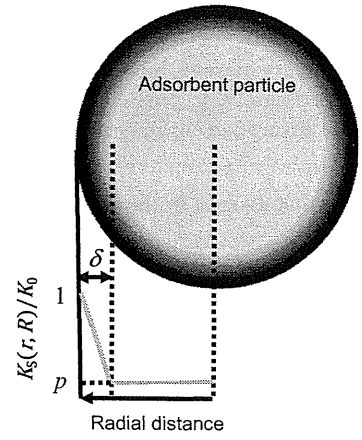

Fig. 3 – Schematic diagram of SAM. Molecules adsorb principally in the exterior region (black region in the figure) close to the particle surface, but to some extent do diffuse into the inner region (light gray region in the figure) of an adsorbent particle. $K_S(r, R)/K_0$, normalized adsorption capacity relative to the adsorption capacity at the external surface linearly decreases with distance from the external surface to a depth δ, (from black to dark gray region) in the figure and thereafter (light gray region) it remains constant as p.

Eq. (5) evolved from the following reasoning: If adsorption occurs only at external particle surface, then adsorption capacity increase is inversely proportional to adsorbent particle size (slope of log q_{50} vs. log $d_{50} = -1$). However, slopes for data points (Fig. 2) range only from −0.34 to −0.58 (less steep than −1), thereby indicating that some of the interior region of the adsorbent particles is available for adsorption. Some adsorbate molecules probably diffuse into and adsorb onto the interior region, while other molecules adsorb onto the exterior region close to the particle outer surface (shell region).

The final form of the isotherm equation, referred to hereinafter as the Shell Adsorption Model (SAM) equation, is expressed as Eq. (6)

$$q_E = C_E^{1/n}\frac{3K_0}{R^3}\int_0^\infty\left\{\int_0^R\left[\max\left(\frac{r-R+\delta}{\delta},0\right)(1-p)+p\right]r^2dr\right\}f_R(R)dR \quad (6)$$

We have applied this SAM equation to describe isotherm data shown in Fig. 1; in doing so, we sought a single set of isotherm parameter values for K_0, n, δ, and p in order to obtain the best model fit to data for PSS adsorption isotherms of SPACa-T, SPACb-T, SPACc-T, SPACd-T, and PAC-T. SAM satisfactorily described the experimental data, as shown in Figs. 1 and 2. Our SAM equation is a modified version of the Freundlich equation that is extended so that the slope in the log–log plot of solid-phase concentration vs. liquid-phase concentration is identical for each of the activated carbon preparations. However, experimentally measured slopes for SPACa-T and SPACb-T were actually slightly less steep than those for SPACd-T and PAC-T when applying the Freundlich

equation to data for each activated carbon (see dashed lines in Fig. 1 and Table 1). Because the change in slope after pulverization was not very marked, however, we feel that the SAM approach was successful in providing a first estimate of the dependence of adsorption capacity on particle size.

3.2. *Adsorption kinetics in the shell adsorption model*

We analyzed adsorption kinetics data to determine whether incorporation of the SAM equation into an adsorption kinetic model adequately describes the kinetics data. In combining the kinetic model with SAM, we used the pore diffusion model (PDM, e.g., Sontheimer et al., 1988). Although the homogeneous surface diffusion model (HSDM) is more widely used than PDM (Sontheimer et al., 1988), we felt that it could not be applied because it assumes homogeneity inside activated carbon particles. Such homogeneity implies that adsorbed molecules have migrated into adsorbent particles by Fick's first law of diffusion according to a local solid-phase concentration gradient, and that adsorbate molecules are ultimately distributed evenly along an adsorbent gradient such that local solid-phase concentrations become equal. Such a scenario is inconsistent with SAM. Therefore, instead of HSDM, we used PDM in which migration of molecules in the liquid-filled pores contributes to transport of adsorbates into particles, while local solid-phase and liquid-phase concentrations in pores remain at equilibrium during the entire period of adsorption (instantaneous adsorption). At an adsorption equilibrium condition in PDM, local liquid-phase concentrations become equal, while local solid-phase concentrations do not necessarily become equal; that condition does not violate SAM. Local adsorption equilibrium is expressed by Eq. (7), as follows:

$$c(t,r,R) = \left(\frac{q(t,r,R)}{K_S(r,R)}\right)^n \tag{7}$$

where t is adsorption time in the batch system (s); $c(t, r, R)$ is the liquid-phase concentration in an adsorbent particle having radius R at radial distance r and time t (mg/L); and $q(t, r, R)$ is the solid-phase concentration in an adsorbent particle having radius R at radial distance r and time t (mg/g).

Diffusion of adsorbate molecules in an adsorbent particle is expressed by Eq. (8), as follows

$$\frac{\partial q(t,r,R)}{\partial t} = \frac{D_P}{\rho}\frac{1}{r^2}\frac{\partial}{\partial r}\left(r^2\frac{\partial c(t,r,R)}{\partial r}\right) \tag{8}$$

where D_P is the pore diffusion coefficient (cm^2/s); and ρ is adsorbent particle density (g/L).

Table 1 – Equilibrium and kinetic parameters and E_{NS} values.

PSS-4600	Simulation 1	Simulation 2	Simulation 3
Adsorption equilibrium	SAM $K_0 = 1.8 \times 10^2$ (mg/g)/(mg/L)$^{1/n}$ $1/n = 0.10$ $\delta = 0.22$ μm $p = 0.038$	Freundlich K (SPACa-T) = 110 (mg/g)/(mg/L)$^{1/n}$ 1/n (SPACa-T) = 0.064 K (SPACd-T) = 39 (mg/g)/(mg/L)$^{1/n}$ 1/n (SPACd-T) = 0.26 K (PAC-T) = 18 (mg/g)/(mg/L)$^{1/n}$ 1/n (PAC-T) = 0.27	
Adsorption kinetics	PDM $D_P = 2.9 \times 10^{-10}$ cm^2/s	HSDM $D_S = 3.3 \times 10^{-13}$ cm^2/s	PDM $D_P = 1.7 \times 10^{-9}$ cm^2/s
E_{NS}	0.25	−2.1	−0.49
PSS-1800	**Simulation 1**	**Simulation 2**	**Simulation 3**
Adsorption equilibrium	SAM $K_0 = 3.2 \times 10^2$ (mg/g)/(mg/L)$^{1/n}$ $1/n = 0.15$ $\delta = 0.20$ μm $p = 0.095$	Freundlich K (SPACa-T) = 190 (mg/g)/(mg/L)$^{1/n}$ 1/n (SPACa-T) = 0.11 K (SPACd-T) = 85 (mg/g)/(mg/L)$^{1/n}$ 1/n (SPACd-T) = 0.28 K (PAC-T) = 45 (mg/g)/(mg/L)$^{1/n}$ 1/n (PAC-T) = 0.28	
Adsorption kinetics	PDM $D_P = 7.6 \times 10^{-10}$ cm^2/s	HSDM $D_S = 2.1 \times 10^{-13}$ cm^2/s	PDM $D_P = 3.2 \times 10^{-9}$ cm^2/s
E_{NS}	0.85	0.11	0.71
PSS-1000	**Simulation 1**	**Simulation 2**	**Simulation 3**
Adsorption equilibrium	SAM $K_0 = 2.8 \times 10^2$ (mg/g)/(mg/L)$^{1/n}$ $1/n = 0.21$ $\delta = 0.21$ μm $p = 0.18$	Freundlich K (SPACa-T) = 190 (mg/g)/(mg/L)$^{1/n}$ 1/n (SPACa-T) = 0.16 K (SPACd-T) = 97 (mg/g)/(mg/L)$^{1/n}$ 1/n (SPACd-T) = 0.27 K (PAC-T) = 67 (mg/g)/(mg/L)$^{1/n}$ 1/n (PAC-T) = 0.28	
Adsorption kinetics	PDM $D_P = 11.0 \times 10^{-10}$ cm^2/s	HSDM $D_S = 1.5 \times 10^{-13}$ cm^2/s	PDM $D_P = 3.3 \times 10^{-9}$ cm2/s
E_{NS}	0.40	−0.84	0.083

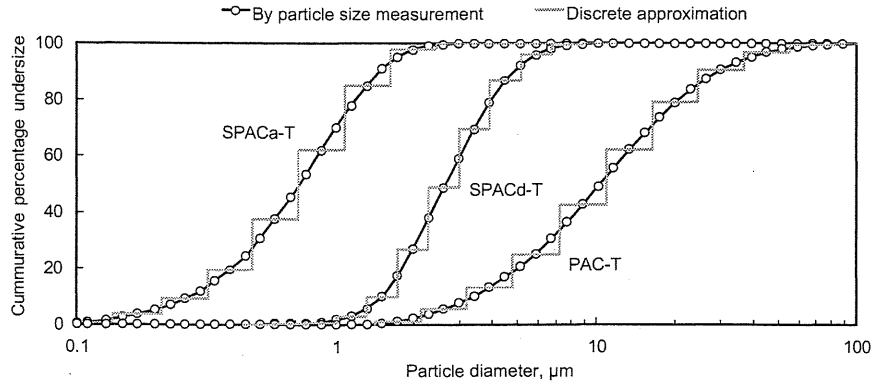

Fig. 4 – Particle size distributions of SPACa-T, SPACd-T, and PAC-T.

External film balance is described by equating mass balance and mass transfer from the external particle surface to inside the particle, as shown in Eq. (9):

$$\frac{d}{dt}\left[\int_0^R r^2 q(t,r,R)dr\right]\frac{1}{R^2}=\frac{k_f}{\rho}[C(t)-c(t,R,R)] \tag{9}$$

where k_f is the liquid film mass transfer coefficient (cm/s), ρ is the adsorbent particle density (g/L), and C(t) is the adsorbate concentration in the bulk water phase as a function of time, t (mg/L).

When considering adsorbent particle size distribution (Matsui et al., 2003), the mass balance equation for an adsorbate in a batch reactor is given in Eq. (10), as follows:

$$\frac{dC(t)}{dt}=-\frac{3C_c k_f}{\rho}\int_0^\infty \frac{f_R(R)}{R}[C(t)-c(t,R,R)]dR \tag{10}$$

We approximated particle size distribution of adsorbent by a discrete density function consisting of M size classes, where M is 13, as shown in Fig. 4. We converted the set of model Eqs (5) and (7)–(10) for adsorption in a batch reactor into a set of ordinary differential equations with respect to time, t, using the method of orthogonal collocation. We took many collocation points in an attempt to describe precisely the change of solid-phase concentration in the vicinity of the particle surface (shell region in Fig. 3). When the number of collocation points was 40, the shell region of a PAC particle 11.8 μm in diameter was divided by 6 in the radial direction and that of a SPAC particle 0.7 μm in diameter was divided by 30. Resultant equations were solved as a system of ordinary differential equations by Gear's stiff method in the IMSL® Math Library, after deriving the analytical Jacobian of the equations (Matsui et al., 2009b). Mass transfer resistance across the liquid film external to the adsorbent particle surfaces was substantially neglected because it cannot be the rate-determining step in well-mixed reactors (Sontheimer et al., 1988). In model simulations, the liquid film mass transfer coefficient (k_f) was set to 10 cm/s, at which value liquid film mass transfer did not control adsorbate uptake to adsorbent, because any values larger than 10 cm/s yielded the same simulation results for concentration decay curves. Finally, a single value of pore diffusion coefficient D_p, the remaining unknown model parameter in PDM, was sought by using quasi-Newton method in the IMSL® Math Library and then the D_p value was determined that produced best-fits to the experimental data for SPACa-T, SPACd-T, and PAC-T under the minimum error criterion [maximizing the E_{NS} value defined by Eq. (11)], as follows:

$$E_{NS}=1-\frac{\sum_{j=1}^{N}\left(C_{obs,j}-C_{cal,j}\right)^2}{\sum_{j=1}^{N}\left(C_{obs,j}-C_{ave}\right)^2} \tag{11}$$

where $C_{obs,j}$ and $C_{cal,j}$ are the observed and calculated concentrations (mg/L) of adsorbate, respectively; C_{ave} is the average concentration of adsorbate (mg/L); and N is the

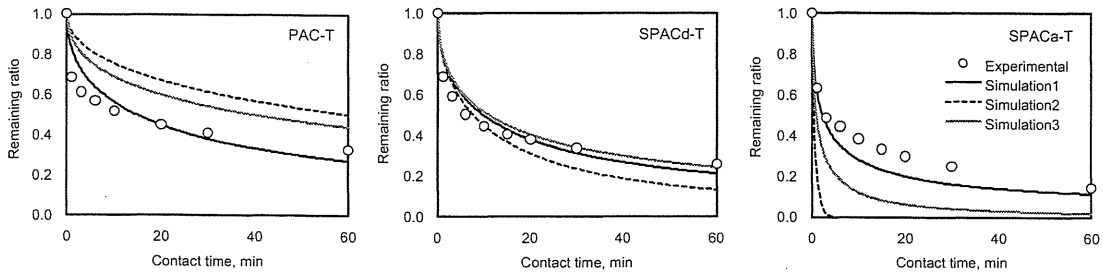

Fig. 5 – PSS-4600 adsorption kinetics data and curves fitted with three models (Initial PSS-4600 concentration was 5 mg/L. PAC-T, SPACd-T, and SPACa-T doses were 500, 200, and 100 mg/L, respectively).

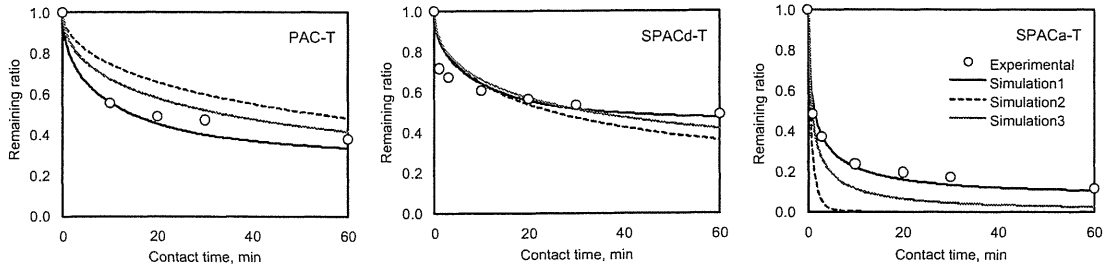

Fig. 6 – PSS-1800 adsorption kinetics data and curves fitted with models (Initial PSS-1800 concentration was 5 mg/L. PAC-T, SPACd-T, and SPACa-T doses were 200, 50, and 50 mg/L, respectively).

number of data points. E_{NS} values vary between $-\infty$ and 1; a value of 1.0 indicates a perfect fit.

As a comparison to the SAM + PDM model (to be called Simulation 1 hereinafter), we used the Freundlich model + HSDM (Simulation 2) and the Freundlich model + PDM (Simulation 3). In these cases, the Freundlich model parameters were individually determined for each activated carbon sample (SPACa-T, SPACd-T, and PAC-T) from the corresponding set of isotherm data. Then, from adsorption kinetics data, a single value for the surface diffusion coefficient D_S was sought under the minimum error criterion to simulate experimental data sets for SPACa-T, SPACd-T, and PAC-T (Simulation 2) [Matsui et al., 2003]. A single value of the pore diffusion coefficient D_P was sought in Simulation 3. Isotherm model parameter values determined from experimental data of Fig. 1 and the D_P and D_S values searched are summarized in Table 1.

All PSS kinetics curves featured a sharp concentration drop in the first few minutes, followed by a subsequent slower decrease (Figs. 5–7). Experimental data for all PSS kinetics are the best described by the SAM + PDM model, into which a single D_P value was inserted. E_{NS} value for PSS-1000, for example, was 0.40 (Table 1). Freundlich model + HSDM simulations carried out with one D_S value (Simulation 2) did not fit experimental data for activated carbons of small and large size: E_{NS} value was −0.84. Freundlich model + HSDM simulations underestimate solute uptake rate into large particle-size adsorbent (PAC-T) and overestimate solute uptake rate into small particle size adsorbent (SPACa-T). Simulation 3, carried out with one D_P value, also did not adequately describe PSS adsorption kinetics for PAC-T and SPACa-T (E_{NS} value was 0.083). Simulation 1 was also reasonable in terms of diffusivity and MW: the smallest molecule, PSS-1000, had the highest diffusivity, followed by PSS-1800; and the largest molecule, PSS-4600, had the lowest diffusivity (the D_P values of PSS-4600, -1800, and -1000 were 2.9×10^{-10}, 7.6×10^{-10}, and 11.0×10^{-10} cm^2/s, respectively; see Table 1). Such a relationship between diffusivity and MW was not observed in Simulations 2 and 3.

In our simulations using the Freundlich model + HSDM and the Freundlich model + PDM, we employed six adjustable parameters (2 model parameters times 3 carbons) to describe adsorption isotherms for the three activated carbon preparations: that is, we determined distinct K and $1/n$ values for SPACa-T, SPACd-T, and PAC-T by linear regression. On the other hand, SAM has four adjustable model parameters for all the three carbons. When considering only the number of adjustable model parameters, the SAM + PDM model should have two less degrees of freedom in describing a variety of adsorption kinetics than the Freundlich model + HSDM or the Freundlich model + PDM. Our results, however, show that SAM + PDM was more accurate in describing adsorption kinetics than the Freundlich model + HSDM or the Freundlich model + PDM. The Freundlich model + HSDM or Freundlich model + PDM simulations underestimate solute uptake rate into the large particle-size adsorbent (PAC-T). Implementation of SAM contributed to the solving this underestimation problem by enhancing adsorbate uptake rate. We attribute this enhancement to the fact that most adsorbate molecules do not diffuse into the inner region of adsorbent particles before reaching adsorption equilibrium. Thus, most of the adsorption process is complete close to the exterior particle surface. Therefore, the superiority of the SAM + PDM model is attributable to the shell adsorption mechanism, and our finding of a better data fit to the SAM + PDM model offers further evidence that PSS molecules adsorb mostly near the adsorbent

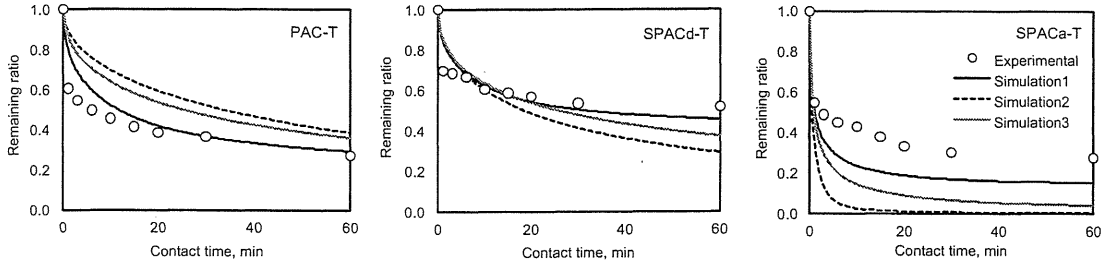

Fig. 7 – PSS-1000 adsorption kinetics data and curves fitted with models (Initial PSS-1000 concentration was 5 mg/L. PAC-T, SPACd-T, and SPACa-T doses were 200, 50, and 50 mg/L, respectively).

particle surface. We believe that the shell adsorption concept provides the best mechanism for describing adsorption kinetics on activated carbons with various particle sizes.

While the discrepancies between the experimental kinetics data and data obtained from Simulation 1 (SAM + PDM) could be partly due to experimental errors, we note some trends. For most experimental data of PAC-T and SPACd-T, concentrations drop rapidly as adsorption begins. However, initial adsorptions were slower in the simulations. On the other hand, the concentrations of SPACa-T for PSS-4600 and -1000 declined faster in the simulations than we observed in our experiments. This pattern of change could be related to local slow diffusion from macropore to micropore, which follows relatively rapid radial diffusion in macropore regions in the adsorbent (Sontheimer et al., 1988; Peel and Benedek, 1980a,b). Adsorption kinetics of a small-MW adsorbate, geosmin, which could adsorb on micropores of SPAC and PAC, is better described by a branched-pore kinetic model (BPKM), in which a slow diffusion mechanism is incorporated into HSDM (Matsui et al., 2009b). We have confirmed that PSS concentration decay curves are also better defined when a slow diffusion mechanism is incorporated into PDM, and the resulting simulation is more successful (data not shown). This improvement may be due to the number of adjustable model parameters for adsorption kinetics increasing from 1 to 3 with implementation of the slow diffusion mechanism.

Further research will be necessary to elucidate the slow diffusion mechanism for PSS adsorption. In this study, we have focused on the fact that application of the shell adsorption mechanism, whereby the compounds we studied adsorb mostly in the vicinity of external adsorbent particle surfaces, dramatically improves modeling of adsorption kinetics as well as isotherms. To enhance our understanding of the adsorption mechanism, we have modeled the adsorption of PSSs which are homogeneous compounds with a defined structure, but with a molecular size similar to that of NOM. In future work, adsorption behavior of NOM must be modeled in order to elucidate its adsorption capacity increase with decreasing adsorbent particle size. However, applying SAM to NOM may be difficult, as NOM is an extremely polydisperse mixture, with MWs ranging from hundreds to tens of thousands. Therefore, the parameter values of δ and p might vary for the various adsorbates with different properties (including MW) within each NOM solution.

The results of the current research may change the paradigm of rapid small-scale column tests (RSSCTs, Crittenden et al., 1986a,b). Our simulation by SAM-PDM implies that adsorption capacity is particle size dependent but that the intraparticle diffusion coefficient is not. The paradigm of SAM-PDM is opposite to that used to scale NOM adsorption in RSSCTs. RSSCTs for NOM adsorption implicitly assume the independence of adsorption capacity from carbon particle size and the proportional diffusivity (PD, the intraparticle diffusion coefficient linearly decreases with particle size). The RSSCT method is well supported by RSSCT data for NOM removal (e.g., Crittenden et al., 1991; Summers et al., 1995). One simple way to reconcile the SAM paradigm with the RSSCT is hypothesising that PAC adsorption capacity is dependent on carbon particle size but that GAC (granular activated carbon) adsorption capacity is not, because GAC has developed macropores that enable PSS and NOM molecules to penetrate inside of carbon particles and which then equalize carbon capacity regardless of carbon particle size (Ando et al., 2010). The diffusivity issue could be resolved if the SAM-PDM would better fit our experimental data when diffusivity was treated as variable rather than constant.

In addition to kinetics, adsorption capacity is a critical parameter that must be considered in the design of RSSCTs (Crittenden et al., 1986a; Sontheimer et al., 1988). Since RSSCTs are conducted on a sieved small-size fraction of crushed carbon particles instead of on the original as-received GAC, which is used in the full-scale adsorber, for proper design of RSSCTs it is essential to understand how not only the adsorption kinetics but also the adsorption capacity is affected by particle size. Actually, capacity increases with decreasing carbon particle size are reported for GACs (Randtke and Snoeyink, 1983; Weber et al., 1983). Moreover, the theoretical background is weak for the PD on which the design of RSSCTs relies. For synthetic organic chemicals (SOCs), on the other hand, isotherm capacities are not affected by carbon particle size (Letterman et al., 1974; Najm et al., 1990 and Leenheer, 2007). The independence of SOC adsorption capacity from carbon particle size is also held for SPAC and PAC (Matsui et al., 2004; Ando et al., 2010). For SOC removals, the RSSCT data well support the assumption of constant diffusivity (Crittenden et al., 1986a). We feel, therefore, that the method of RSSCT design for NOM adsorption could be improved through the study of how NOM adsorption capacity is affected by GAC particle size.

4. Conclusions

1) We have proposed a shell adsorption mechanism by which PSS molecules are principally adsorbed in the exterior (shell) region of activated carbon particles and adsorbed less in the interior region. The increasing adsorption capacity with decreasing particle size is explained by the increase in specific external surface area (surface area per unit mass) available for adsorption with decreasing adsorbent particle size. Therefore, the PSS adsorption capacity of SPAC was higher than that of PAC.
2) We have proposed a new isotherm equation (SAM), which incorporates the shell adsorption mechanism into the Freundlich model, and we have successfully described PSS adsorption isotherms for SPACs and PAC with the same model parameters.
3) PSS adsorption kinetics were described much better by SAM incorporated into PDM than by the conventional approaches of the Freundlich model + HSDM or the Freundlich model + PDM, which further supports our proposed shell adsorption mechanism.

Acknowledgments

This study was supported by a Grant-in-Aid for Scientific Research A (21246083) from the Ministry of Education, Science,

Sports, and Culture of the Government of Japan; by a research grant from the Ministry of Health, Labor, and Welfare; and by Metawater Co., Tokyo, Japan.

Appendix. Supplementary information

Additional details, including Tables 1S, 2S, and 3S and Figures 1S, are available in the online version at doi:10.1016/j.watres.2010.11.020.

REFERENCES

Ando, N., Matsui, Y., Kurotobi, Y., Nakano, Y., Matsushita, T., Ohno, K., 2010. Comparison of natural organic matter adsorption capacities of super-powdered activated carbon and powdered activated carbon. Water Res. 44 (14), 4127–4136.

Crittenden, J.C., Berrigan, J.K., Hand, D.W., 1986a. Design of rapid small-scale adsorption tests for a constant diffusivity. J. Water Pollut. Control Fed. 58 (4), 312–319.

Crittenden, J.C., Berrigan, J.K., Hand, D.W., Lykins, B., 1986b. Design of rapid small-scale adsorption tests for nonconstant diffusivity. J. Environ. Eng.–ASCE 113 (2), 243–259.

Crittenden, J.C., Reddy, P.S., Arora, H., Trynoski, J., Hand, D.W., Perram, D.L., Summers, R.S., 1991. Predicting GAC performance with rapid small-scale column tests. J. Am. Water Works Assoc. 83 (1), 77–87.

Karanfil, T., Kilduff, J.E., Schlautman, M.A., Weber Jr., W.J., 1996a. Adsorption of organic macromolecules by granular activated carbon. 1. Influence of molecular properties under anoxic solution conditions. Environ. Sci. Technol. 30 (7), 2187–2194.

Karanfil, T., Schlautman, M.A., Kilduff, J.E., Weber Jr., W.J., 1996b. Adsorption of organic macromolecules by granular activated carbon. 2. Influence of dissolved oxygen. Environ. Sci. Technol. 30 (7), 2195–2201.

Leenheer, J.A., 2007. Progression from model structures to molecular structures of natural organic matter components. Annals of Environ. Sci. 1, 57–68.

Letterman, R.D., Quon, J.E., Gemmell, R.S., 1974. Film transport coefficient in agitated suspensions of activated carbon. J. Water Pollut. Control Fed. 46 (11), 2536–2547.

Li, Q., Snoeyink, V.L., Mariãas, B.J., Campos, C., 2003a. Elucidating competitive adsorption mechanisms of atrazine and NOM using model compounds. Water Res. 37 (4), 773–784.

Li, Q., Snoeyink, V.L., Mariñas, B.J., Campos, C., 2003b. Three-component competitive adsorption model for flow-through PAC systems. 1. Model development and verification with a PAC/membrane system. Environ. Sci. Technol. 37 (13), 2997–3004.

Matsui, Y., Yuasa, A., Li, F., 1998. Overall adsorption isotherm of natural organic matter. J. Environ. Eng.–ASCE 124 (11), 1099–1107.

Matsui, Y., Fukuda, Y., Inoue, T., Matsushita, T., 2003. Effect of natural organic matter on powdered activated carbon adsorption of trace contaminants: characteristics and mechanism of competitive adsorption. Water Res. 37 (18), 4413–4424.

Matsui, Y., Fukuda, Y., Murase, R., Aoki, N., Mima, S., Inoue, T., Matsushita, T., 2004. Micro-ground powdered activated carbon for effective removal of natural organic matter during water treatment. Water Sci. Tech.: Water Supply 4 (4), 155–163.

Matsui, Y., Murase, R., Sanogawa, T., Aoki, N., Mima, S., Inoue, T., Matsushita, T., 2005. Rapid adsorption pretreatment with submicron powdered activated carbon particles before microfiltration. Water Sci. Tech. 51 (6–7), 249–256.

Matsui, Y., Aizawa, T., Kanda, F., Nigorikawa, N., Mima, S., Kawase, Y., 2007. Adsorptive removal of geosmin by ceramic membrane filtration with super-powdered activated carbon. J. Water Supply: Res. Technol.–AQUA 56 (6–7), 411–418.

Matsui, Y., Hasegawa, H., Ohno, K., Matsushita, T., Mima, S., Kawase, Y., Aizawa, T., 2009a. Effects of super-powdered activated carbon pretreatment on coagulation and trans-membrane pressure buildup during microfiltration. Water Res. 43 (20), 5160–5170.

Matsui, Y., Ando, N., Sasaki, H., Matsushita, T., Ohno, K., 2009b. Branched pore kinetics model analysis of geosmin adsorption on super-powdered activated carbon. Water Res. 43 (12), 3095–3103.

Najm, I.N., Snoeyink, V.L., Suidan, M.T., Lee, C.H., Richard, Y., 1990. Effect of particle size and background natural organics on the adsorption efficiency of PAC. J. Am. Water Works Assoc. 82 (1), 65–72.

Peel, R.G., Benedek, A., 1980a. Attainment of equilibrium in activated carbon isotherm studies. Environ. Sci. Technol. 14 (1), 66–71.

Peel, R.G., Benedek, A., 1980b. Dual rate kinetic model of fixed bed adsorber. J. Environ. Eng.–ASCE 106 (4), 797–813.

Randtke, S.J., Snoeyink, V.L., 1983. Evaluating GAC adsorptive capacity. J. Am. Water Works Assoc. 75 (8), 406–413.

Sontheimer, H., Crittenden, J.C., Summers, R.S., 1988. Activated Carbon for Water Treatment, second ed. DVGW-Forschungsstelle, Karlsruhe, Germany.

Summers, R. Scott, Hooper, Stuart M., Solarik, Gabriele, Owen, Douglas M., Hong, Seongho, 1995. Bench-scale evaluation of GAC for NOM control. J. Am. Water Works Assoc. 87 (8), 69–80.

Weber Jr., W.J., Voice, T.C., Jodellah, A., 1983. Adsorption of humic substances: effects of heterogeneity and system characteristics. J. Am. Water Works Assoc. 75 (12), 612–619.